WATER RESOURCES RESEARCH, VOL. 45, W11408, doi:10.1029/2008WR007370, 2009

Click Here for Full Article

Modeling of high-latitude spring freshet from AMSR-E passive microwave observations

Fenglin Yan,[1] Joan Ramage,[1] and Rose McKenney[2]

Received 18 August 2008; revised 2 July 2009; accepted 28 July 2009; published 11 November 2009.

[1] Snowmelt runoff in high latitudes has significant impacts on global climatic and hydrologic systems. Snowmelt timing and snow water equivalent (SWE) from the Advanced Microwave Scanning Radiometer for EOS (AMSR-E) are inputs to the new flux-based SWEHydro model to simulate the spring streamflow without meteorological data for high-latitude, snow-dominated drainages. The model was developed for the Ross River (7250 km^2) and tested on the Pelly River (49,000 km^2), nested tributaries to the Yukon River. The model uses four parameters: snowmelt rate during and after the melt transition (as defined by passive microwave observations), and flow timing during and after the melt transition. A normalized mismatch function was used to calculate the error compared with observed discharge. Curves were ranked by lowest error in freshet timing, peak timing, and magnitude. Melt timing is a good predictor of freshet timing across years and basins. The system is most sensitive to the flow timing after the transition.

Citation: Yan, F., J. Ramage, and R. McKenney (2009), Modeling of high-latitude spring freshet from AMSR-E passive microwave observations, *Water Resour. Res.*, *45*, W11408, doi:10.1029/2008WR007370.

1. Introduction

[2] Snow extent, snow water equivalent (SWE), and the spring snowmelt timing have a strong influence on hydrological systems from local to continental scales [*Chang et al.*, 2003]. This is particularly important in high-latitude watersheds such as the Yukon, which flows into the Bering Sea, a major biologically productive waterway feeding the Arctic Ocean [e.g., *Grebmeier et al.*, 2006; *Aagaard and Carmack*, 1989]. The field of snow monitoring made progress three decades ago using passive microwave remote sensing techniques [e.g., *Chang and Gloersen*, 1975; *Chang et al.*, 1976, 1987]. More recent work has improved detection and analysis of snow extent [e.g., *Hall et al.*, 1991; *Armstrong and Brodzik*, 2001], SWE [e.g., *Chang et al.*, 2003; *Kelly et al.*, 2003; *Derksen et al.*, 2008], and melt [*Ramage et al.*, 2006; *Apgar et al.*, 2007; *Tedesco*, 2007]. Existing snowmelt runoff models tend to depend on meteorological information which is scarce in most remote, high-latitude, or alpine basins [e.g., *Martinec and Rango*, 1986; *Schmugge et al.*, 2002; *Woo and Thorne*, 2006]. However, there is still a major gap in monitoring the relationship between snowmelt and stream runoff, especially in remote, high-latitude regions and ungauged watersheds [*Woo and Thorne*, 2006; *Marsh et al.*, 2008]. An understanding of the snow distribution, snowmelt, and associated runoff characteristics and their incorporation into hydrological models is significant for a wide array of atmospheric, hydrological, and ecological models [*Liston*, 1999].

[3] The freshet, or flow associated with thawing snow and ice in northern basins, is an important component of high-latitude hydrology. This paper presents a modeling method to reconstruct the freshet and spring streamflow characteristics solely based on passive microwave remote sensing and digital elevation model (DEM) data (Table 1) without any field measurements (average base flow was also an assumed input value for the test basins). Thus it is not necessary to have meteorological information to run this model. We first tested the model (SWEHydro) in two gauged basins, the Ross River basin (7,250 km^2), a nested subwatershed of the Pelly River basin, and the Pelly River basin above Faro (21,000 km^2) and then applied the model to the larger Pelly River above Pelly Crossing (49,000 km^2), a large undammed, gauged tributary to the Yukon River.

[4] The Advanced Microwave Scanning Radiometer for EOS (AMSR-E) sensor is an EOS mission instrument launched aboard NASA's Aqua satellite on 4 May 2002. It has 12 channels at six frequencies (6.925, 10.65, 18.7, 23.8, 36.5, and 89 GHz) and dual-polarization [*Kawanishi et al.*, 2003]. AMSR-E generally has more than two observations per day in arctic and subarctic regions, and up to eight observations near the poles (http://nsidc.org/data/tools/pmsdt/as2gt.html). We used 18.7- and 36.5-GHz frequency AMSR-E observations to obtain the snowmelt timing and SWE for this study.

[5] The Pelly River basin is located at the southeastern part of the Yukon River basin, covering an area of 49,000 km^2, and contains three long-term Environment Canada gauges: near the mouth of the Ross River, on the Pelly River below Vangorda Creek (near Faro), and on the Pelly River at Pelly Crossing (Figure 1, Table 2). The Pelly River basin has a wide range of elevations, ecosystems, and climates, with significant variations in atmospheric patterns [*Brabets et al.*, 2000; *Ramage et al.*, 2007], which make it especially sensitive to climatic and hydrological change. This

[1]Earth and Environmental Sciences Department, Lehigh University, Bethlehem, Pennsylvania, USA.
[2]Department of Geosciences/Environmental Studies, Pacific Lutheran University, Tacoma, Washington, USA.

Copyright 2009 by the American Geophysical Union.
0043-1397/09/2008WR007370$09.00

Table 1. Data Used in the SWEHydro Model

Data	Frequency	Spatial Resolution	Data Source
AMSR-E[a] L3 daily snow water equivalent	18.7, 36.5 GHz	25 km	NSIDC[b]
AMSR-E L2A brightness temperature	36.5 GHz	25 km	NSIDC
Digital elevation model	NA[c]	90 m	Environment Yukon

[a]Advanced Microwave Scanning Radiometer for EOS.
[b]National Snow and Ice Data Center.
[c]Not applicable.

basin was chosen because of the varied terrain and the presence of gauged, nested basins that can be used to quantify SWE, snowmelt, and discharge relationships on a range of scales.

[6] This research aims to provide a way to simulate stream runoff in inaccessible mountainous regions and ungauged watersheds with sparse meteorological data, a limitation in many northern watersheds [*Marsh et al.*, 2008], so no dynamic field measurements were used as input data. This model output is based solely on microwave remote sensing observations and 1:250,000 (90 m) DEM. Ground observations were used to test the model and select the best fit model parameters. Satellite data are currently freely available from the National Snow and Ice Data Center (NSIDC) so the method could be implemented for all high-latitude basins relatively inexpensively.

2. Data

2.1. AMSR-E Level 2A Daily Brightness Temperature

[7] The AMSR-E level 2A daily brightness temperature (T_b) data gridded to 25 × 25 km^2 spatial resolution

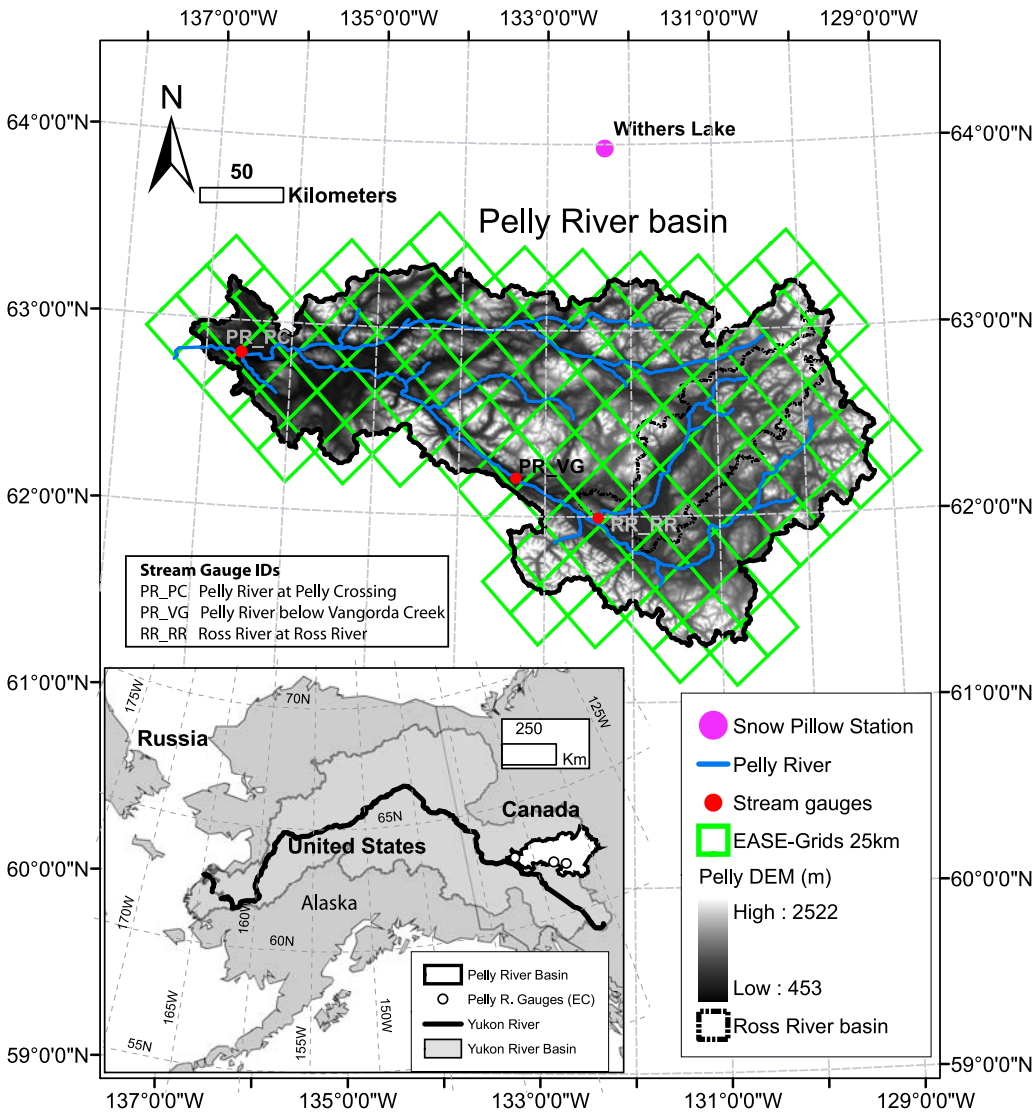

Figure 1. Detailed digital elevation model (DEM) of the Pelly River basin with a 25 km × 25 km EASE-Grid superimposed on top. Ross River, a tributary of the Pelly River, has a thin dashed outline. The Withers Lake snow pillow is shown just to the north of the basin, and the three gauges used in this study are shown as red dots. Inset shows location of the Yukon River and Pelly River basins.

Table 2. Data Used to Compare With SWEHydro Model Output

Identification	Latitude (deg)	Longitude (deg)	Station Elevation (m above sea level)	Drainage Area (km^2)	Source
Pelly River at Pelly Crossing, Yukon Territory	62.83	−136.58	458	49,000	Water Survey/Environment Canada
Pelly River below Vangorda Creek, Yukon Territory	62.22	−133.37	633	22,100	Water Survey/Environment Canada
Ross River at Ross River, Yukon Territory	61.99	−132.37	685	7,250	Water Survey/Environment Canada
Withers Lake Snow Pillow Station,Yukon Territory	63.98	−132.30	975	NA	Yukon Territorial Government/ Environment Yukon

[*Ashcroft and Wentz*, 2003] were used to extract the snowmelt timing for each pixel from 2003 to 2006. The raw AMSR-E L2A data were first processed using the AMSR-E Swath-to-Grid Toolkit (AS2GT) in the Passive Microwave Swath Data Tools (PMSDT) provided by the NSIDC. Then an Interactive Data Language (IDL) program was used to extract and process data to determine the snowmelt onset and the spring snowmelt transition period using the techniques of *Apgar et al.* [2007] and *Ramage et al.* [2007]. Ground-based measurements such as near-surface air temperature and snow wetness were used to determine the melt thresholds [*Apgar et al.*, 2007]. Air temperature was collected hourly using a HOBO® temperature logger. Stations are located on the north (shady) side of a spruce tree under a wooden shelf to reduce the impact of precipitation (see *Apgar et al.* [2007] for observations and detailed methods). Wetness measurements of surface and near-surface snow were collected during field campaigns in 2005, 2006, and 2007 using a snow capacitance probe. Field observations are not shown here. Snowmelt onset for AMSR-E 37-GHz vertically polarized data are determined by the simultaneous occurrence of T_b greater than 252 K and diurnal amplitude variations (DAV) greater than ±18 K [*Apgar et al.*, 2007]. For this area, daily observations occur at 1250–1330 PST (day) and 0300–0400 PST (night); DAV are the running difference of the morning and evening observations, where observations within 1 hour of each other are averaged (Figures 2a and 2b). These observations were used to determine the melt characteristics of the snowpack in order to constrain melt rates and intervals in the model.

2.2. AMSR-E Level 3 Daily SWE

[8] The AMSR-E level 3 daily SWE data with a 25 × 25 km^2 spatial resolution [*Kelly et al.*, 2004] were used to estimate the total mass of snow on the ground from 2003 to 2006. The algorithms are based on the fact that the deeper the snow, the more scatterers there are, and therefore more scattering occurs to attenuate the signal [*Mätzler*, 1987; *Foster et al.*, 1991]. Snow depth and snow water equivalent algorithms were developed over the past few decades [e.g., *Kunzi et al.*, 1982; *Chang et al.*, 1982; *Hallikainen and Jolma*, 1986; *Goodison et al.*, 1990]. The current algorithm for the SWE product is based on work by *Chang et al.* [1987, 1997] with ongoing updates (see http://nsidc.org). The probability of snow is derived from *Dewey and Heim* [1981]. If snow is likely, data are processed to determine if snow is present. Snow is present if $T_b36V \leq 255$ K and $T_b36H \leq 245$ K. The SWE algorithm uses AMSR-E L2A brightness temperature data to calculate the snow depth from each frequency less than 89 GHz, averages them, and then the average snow depth is converted to SWE with snow density data. For shallow snow, the snow depth was estimated as 5.0 cm. For medium to deep snow, the snow depth was calculated from the following equation:

$$SD = (ff \times (SD_f)) + ((1 - ff) \times (SD_o)), \quad (1)$$

where SD_f is the snow depth from forested area; SD_o is the snow depth from nonforested area; ff is the forest fraction. Forest fraction and forest density come from Moderate Resolution Imaging Spectroradiometer (MODIS) data [*Hansen et al.*, 2003]. Snow density is based on that of *Sturm et al.* [1995]. On the basis of snow depth, SWE can be calculated as

$$SWE = SD(cm) \times density\left(g\,cm^{-3}\right) \times 10.0(mm). \quad (2)$$

[9] We used the HDF-EOS Image Tool provided by NSIDC to extract SWE observations from the AMSR-E level 3 data (Table 1, Figure 2c). Remotely sensed SWE is well understood for certain homogeneous regions such as the Canadian prairies [e.g., *Walker and Goodison*, 1993], but it is difficult to get an accurate estimation in the boreal forest or other heterogeneous terrain [*Derksen et al.*, 2008]. The global SWE algorithm for AMSR-E level 3 data [*Kelly et al.*, 2004] are the best available regional data to date. However, global algorithms are not appropriate for all sites [*Schmugge et al.*, 2002] and there is usually an underestimation of actual SWE [*Dong et al.*, 2005]. Therefore we assume that the global SWE algorithm used here provides a minimum value of snow water equivalent in the Pelly River basin. We use the premelt SWE estimated as the maximum SWE value at snowmelt onset date ±5 days as the model input (Figures 2c and 2d).

2.3. Digital Elevation Model

[10] The 1:250,000 (90 m) digital elevation model (DEM) (http://www.environmentyukon.gov.yk.ca/geomatics/data/90m_dem.html) was processed in ArcMap and ArcHydro to outline the watershed boundary and terrain parameters (Figure 1). In future model versions the DEM will also be used to better characterize the flow path and distance.

2.4. Hydrometric Data

[11] The hydrological records of three Environment Canada gauges from 2003 to 2006 were used to approximate the average base flow (an input to the model) and to compare daily discharge with model output. Discharge data come from monitoring station 09BA001 at the "Ross River near Ross River," located at 61°59′40″N, 132°22′40″W; station 09BC004, "Pelly River below Vangorda Creek," located at 62°13′20″N, 133°22′40″W; and station 09BC001, "Pelly River at Pelly Crossing," located at 62°49′47″N,

136°34′50″W (Table 2, Figure 1). Base flow values were based on the winter average for the period of interest; the low flows are a small component of the discharge once melting starts.

2.5. Snow Pillow Data

[12] Snow pillow data recorded at the Withers Lake station (corresponding to equal-area scalable Earth (EASE) coordinates 275, 282 (63.7648°N, 132.541°W)) were used

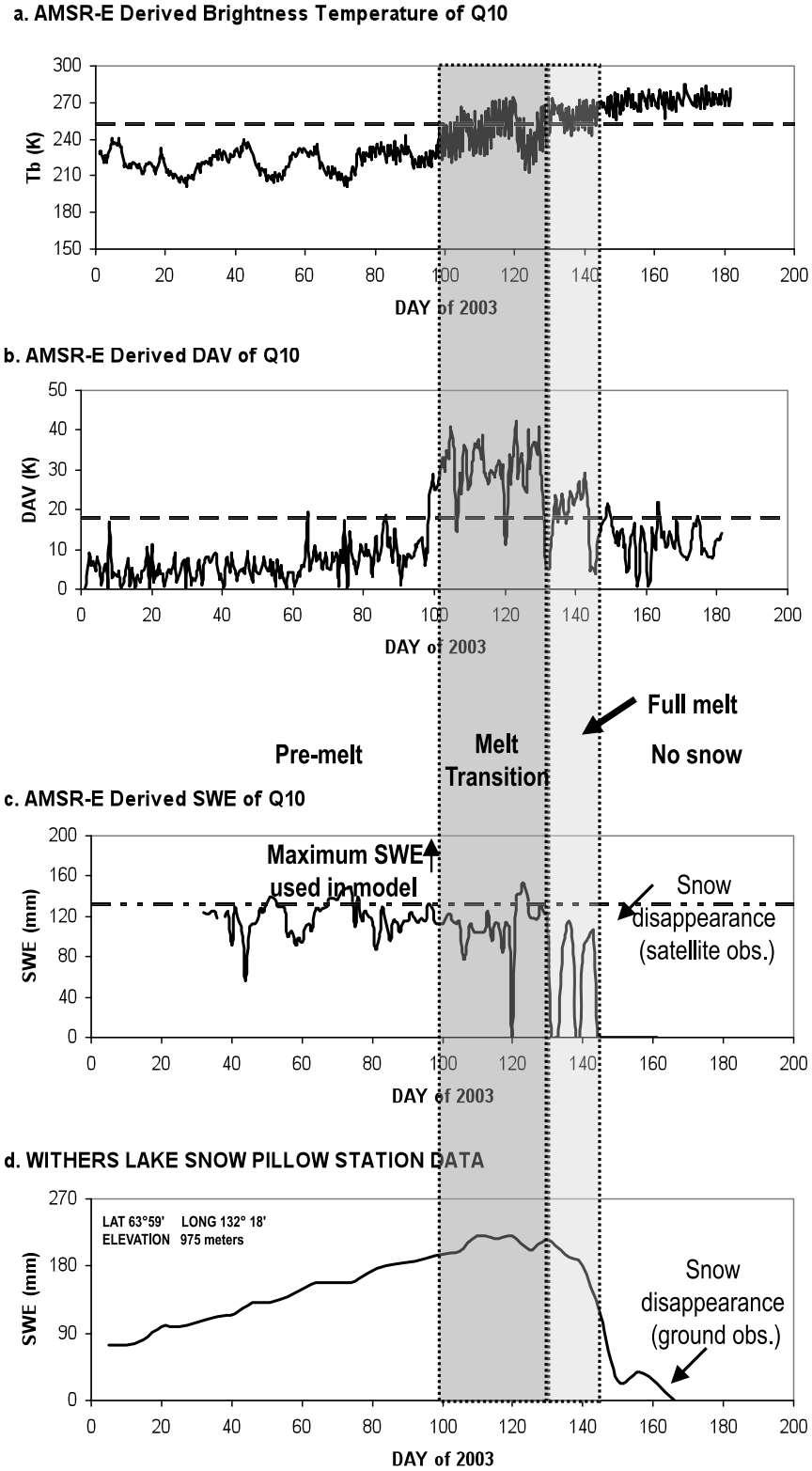

Figure 2

Table 3. Parameters Used in the SWEHydro Sensitivity Tests[a]

Trial	Smr1 (mm/d)	Smr2 (mm/d)	Ft1 (days)	Ft2 (days)
a	**0.1–0.9 (0.2)**	10	8	2
b	0.5	**8–12 (1)**	8	2
c	0.5	10	**6–10 (1)**	2
d	0.5	10	8	**1–5 (1)**

[a]Bold ranges indicate the parameter that was varied for each test. Other values were held fixed for that test.

Table 4. Parameter Ranges for Monte Carlo Simulations

	Smr1	Smr2	Ft1	Ft2
Range	0–1 mm/d	8–12 mm/d	6–10 days	1–5 days
Constraints	floating	floating	integer	integer

to evaluate the satellite SWE data for this region. Data were collected by the Yukon Territorial Government daily (see Yukon Snow Survey Bulletin, http://www.environmentyukon.gov.yk.ca/monitoringenvironment/snow_survey.php).

3. Methods

3.1. SWEHydro Model

[13] We developed the SWEHydro model to quantitatively determine the relationship between snow distribution on the landscape, snowmelt timing, and spring stream runoff in high-latitude and high-altitude basins. Here we describe the assumptions, procedures, limitations, and advantages. We ran a set of sensitivity tests and developed a Monte Carlo approach to determine values that optimize the parameters for each basin. This model does not depend on ground-based observations of snowpack or meteorological information. Thus we made several assumptions. Future work may make it possible to refine or reduce these assumptions. Ground-based observations of the daily streamflow from the Water Survey of Environment Canada (http://www.wsc.ec.gc.ca/hydat/H2O/) were used to help determine whether the model is a good representation of the snowmelt runoff. If parameters can be estimated for ungauged basins, the technique could be effective in ungauged basins.

3.1.1. Assumptions

[14] This model has several assumptions. The first assumption is that snow accumulates to its maximum amount before the snowmelt onset. In reality, the SWE may lose some mass prior to melt due to sublimation or short melt events or accumulate wet snow after the melt initiation. However, the passive microwave SWE algorithms do not interpret postmelt-initiation SWE effectively, so the model is limited to the premelt SWE. Because of the inaccurate SWE estimations for AMSR-E data during the melt season, we define premelt SWE as maximum SWE at the snowmelt onset date ±5 days as the model input. The wet snow that accumulates after this date is ignored in the model, but it is usually not a large part of the total mass accumulation in this area (Figure 2d).

[15] The second and third assumptions relate to how fast the snow melts at different stages, during and after the snowmelt transition period. We define a transition period that starts at the AMSR-E derived snowmelt onset date and ends at the end of the high DAV period (Figure 2). We assume that the snowpack melts slowly during the transition period (smr1), and we have observed that the snowpack melts during the day and refreezes at night. Because the air temperature is usually below zero at this stage, the melt is mostly confined to the surface and meltwater probably refreezes within the snowpack. Values for smr1 are lower than for smr2. We assume that the snowpack melts at a faster average rate after the transition period (smr2). It melts day and night. Snowmelt rate 2 was initially derived from the *U.S. Army Corps of Engineers* [1956] equation (smr2 (mm/d) = 2.286 × T_{mean} (Celsius)), assuming a mean temperature of 4°C. Subsequently, we varied the average rate from 8 to 12 mm/d. See Tables 3 and 4 for values used for snowmelt rates. We assume that all snow runs off. Thus sublimation is neglected (discussed above) and infiltration is assumed to be negligible. This is a reasonable assumption for this region and this time of year due to the presence of permafrost and seasonally frozen ground.

[16] We assumed flow rates for meltwater during and after the transition period. We assumed that water flows slowly during the transition period (ft1). The water flows within a still frozen snowpack and on seasonally frozen ground, and it might be refrozen at night. After the transition period, meltwater flows much faster (ft2) in the snowpack and channel. The water is not trapped by frozen ice after the transition period. We recognize that this parameter encapsulates multiple processes and scales, and thus future work will involve building an understanding of how the parameter varies with basin characteristics. See Tables 3 and 4 for values used. Flow timing is in pixels per day to facilitate working with coarse-resolution data and for model output to be portrayed as a daily hydrograph.

[17] Finally, stream base flow was summarized from historical streamflow records as the average winter low

Figure 2. Examples of Advanced Microwave Scanning Radiometer for EOS (AMSR-E) derived snowmelt timing and snow water equivalent (SWE) for a Yukon River basin pixel (Q10) located at 63.7648°N, 132.541°W (EASE-Grid coordinates (275, 282)), compared with the corresponding snow pillow SWE measurement at Withers Lake. (a) Daily AMSR-E brightness temperature (Tb). (b) Diurnal amplitude variations (DAV). When T_b are greater than 252 K and DAV are greater than ±18 K, the snowpack is melting [*Apgar et al.*, 2007]. The spring melt transition season of 2003 began on day 102 and ended on day 130 (shaded in darker gray). More intense melt at the end of the transition is highlighted in lighter gray. (c) AMSR-E derived daily SWE. Four distinct time periods are labeled based on melt timing: premelt (no melt), transition period (mild melt), full melt, and no snow. When snowpack starts to melt, moisture will make the SWE data unreliable [*MacKay et al.*, 2006]. We use the maximum SWE at snowmelt onset date ±5 days as the maximum SWE for the whole year (shown as vertical arrow). (d) SWE from Withers Lake snow pillow station shows ground-based accumulating SWE until approximately the end of transition period. The ground-measured SWE has a higher value than the AMSR-E derived SWE, and a later snow disappearance day.

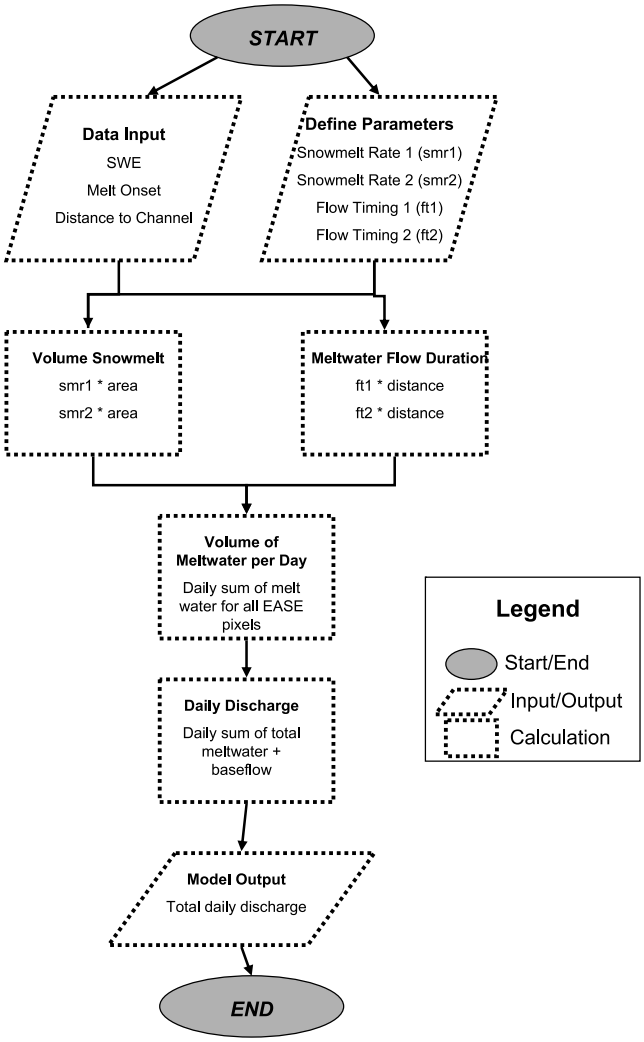

Figure 3. Flowchart of SWEHydro model.

flow (1 January to 15 March, 1989–2004). From the Environment Canada discharge records, the base flow of the Ross River at Ross River is 8 m^3/s; the Pelly River below Vangorda Creek (Faro) is 27 m^3/s, and the Pelly River at Pelly Crossing is 60 m^3/s. Base flow is added to runoff to generate the model hydrograph. Base flows are a small to negligible component of the peak flows, ranging from 2.5 to 5% on the Pelly River for this period.

3.1.2. Modeling Procedures

[18] The basic idea of this model is to map the snow distribution, simulate the volume of released water per day for each pixel based on satellite observations of melt onset and transition to more intense melting, and then to add the water volume and flow distance for all pixels to base flow to generate the overall basin hydrograph. The detailed steps follow (Figure 3).

[19] For each pixel at the EASE-Grid 25 km × 25 km resolution there were three steps. The first step was to determine input data. Input data were (1) the snowmelt onset date (the beginning of the melt transition period), (2) the end of high DAV, which corresponds to the end of the melt transition period and the beginning of intense melting, (3) the maximum SWE at the snowmelt onset date ±5 days, and (4) base flow (from historical data). Specifics about obtaining input values are discussed in section 2.

[20] The second step was to calculate the volume of water released for different intervals, specifically based on melt rates during and after the transition period until the SWE reaches zero. The volume of released water per day is the product of snowmelt rate and the pixel area.

[21] The third step was to determine the lag time between melt and arrival at the channel to determine flow timing. We used the number of EASE-Grid pixels meltwater would flow across to the channel and converted it to distance. This step will be refined, but is useful as a first approximation at the same scale as the input data.

[22] The procedure is to calculate the volume of snowmelt for each pixel and day and determine the meltwater flow duration to the gauge for each pixel. Then the meltwater reaching the gauge for each day is added to the winter base flow to determine discharge. The snowmelt rate changes between the transition period and the full melt period (smr1 and smr2, respectively), and the flow timing also changes when the melt state progresses (ft1 and ft2, respectively). The following equation shows the components used to calculate discharge at the gauge:

$$Q_j = B + \sum_{j=1}^{365} \sum_{i=1}^{n} SMR_{(i,j-k_i)} * A_i, \tag{3}$$

for all j and i where SWE > 0 and where Q = total discharge at gauge ($m^3\ s^{-1}$), B = base flow, assumed based on historical winter average flows ($m^3\ s^{-1}$), i = pixel index, j = day of year, SMR = snowmelt rate based on satellite observations of melt state of snow (mm/(1000 × d)), n = total number of pixels in drainage basin, k_i = days for meltwater to reach the gauge (varies by pixel and year) calculated as FT × D where FT is flow timing (days/pixel) and D is distance (pixels), and A_i = pixel area within basin.

[23] This equation is deceptively simple because smr and ft selection are based on a complex interpretation of satellite data. Once input, melt, and lag time details have been calculated for the individual pixels, they need to be compiled into a basin response. First, the model adds the volume of released water up for each day and pixel and uses the pixel distance and DEM to determine the simplified flow routing. Then, the model converts the total volume of water reaching the stream per day to discharge (m^3/s). For the gauged basins shown here, we then compare modeling results with actual discharge observations.

3.1.3. Limitations and Advantages

[24] There are some limitations in this model that restrict the accuracy of the model estimates, as well as some advantages. The coarse resolution of the passive microwave input data is a source of error. AMSR-E data can be converted to EASE-Grid format 12.5 and 25 km, too low to investigate snow distribution precisely in the research area, compared with visible and infrared images. Second, the AMSR-E-derived SWE information is not yet very reliable for this region because of the heterogeneous terrain and lack of extensive ground truth. Note that efforts are being made to improve SWE retrievals in this area (R. E. J. Kelly, personal communication, 2008). In addition, SWE data are not accurate after the initial snowmelt [*Walker and*

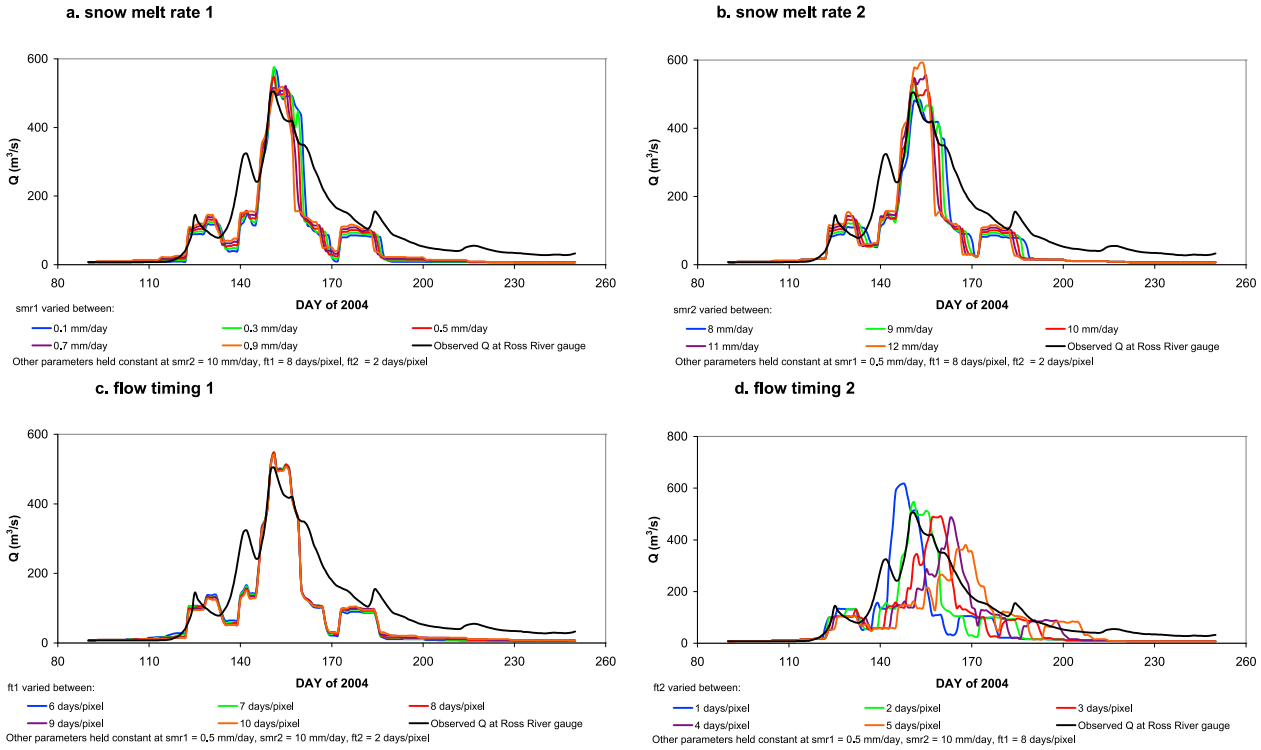

Figure 4. Sensitivity tests of model parameters (a) smr1, (b) smr2, (c) ft1, and (d) ft2. Variations of smr1 and ft1 do not have much effect on the hydrographs. Varying smr2 affects the peak discharge magnitude. Varying ft2 affects both peak timing and magnitude. The larger ft2 is, the lower the peak magnitude and the later the peak time (Figure 4d).

Goodison, 1993]. SWE algorithms usually underestimate the actual snow amount [e.g., *Dong et al.*, 2005; *MacKay et al.*, 2006]. The underestimation is consistent with our field observations in this region. The lack of local groundwater information is also a limitation. The interactions between stream water and groundwater in the research area are unknown for most of the basin; and infiltration rate is hard to determine and likely to be highly variable. The accessibility to most of the research area is limited in winter and spring. It is difficult to get in situ snow information and difficult to correlate the detailed field measurements across scales to the real, varied conditions of a whole 25 × 25 km^2 pixel.

[25] Despite these limitations, the remotely sensed data and modeling approach also have advantages. Microwave data used for both the SWE determination and the melt onset timing are effective in darkness and in cloud-covered conditions. The multiple observations per day of passive microwave data offer a distinct advantage over visible and infrared sensors, as well as over active microwave data, because they can be used to monitor dynamic processes that are highly responsive to atmospheric variability such as snowmelt. The data sets provide a consistent and long-term (2002 to present for AMSR-E, longer for other sensors) daily record of remote areas, a comprehensive data set difficult to achieve with sparse ground-based measurements. Because this is a region with little meteorological data available, especially in real time, the model was developed in such a way as not to depend on it, a clear advantage at sites without it (see, e.g., the predictions in ungauged basins Web site (http://pub.iwmi.org/UI/Content/Default.aspx?PGID = 0)).

3.2. Sensitivity Tests

[26] In order to run the model, values for four parameters must be determined: snowmelt rate during (smr1) and after (smr2) the melt transition (Figure 2) and flow timing (the rate meltwater flows to the gauge) during (ft1) and after (ft2) the melt transition. Sensitivity tests were used to examine how each of the four parameters, smr1, smr2, ft1, and ft2, influenced the simulated hydrographs. Three parameters were held fixed and only one parameter was varied at a time to examine its effect. Ross River basin in 2004 was simulated for this purpose. The results were applied to simulations of other years and basins because all three of these basins are large basins, so they are likely to have comparable scaling parameters. Preliminary work with much smaller basins suggests that the model works well there too. Ranges for each parameter were estimated based on the range of physical processes encapsulated by the parameter and empirical observations. In the sensitivity tests, smr1 was varied from 0.1 to 0.9 mm/d at 0.2 mm/d increments; smr2 was varied from 8 to 12 mm/d at 1 mm/d increments; ft1 was varied from 6 to 10 d/pixel at 1 d/pixel increments; ft2 was varied from 1 to 5 d/pixel at 1 d/pixel increments (Figure 4, Table 3).

3.3. Monte Carlo Simulations

[27] The Monte Carlo method is a computational algorithm based on repeated random sampling of variables to compute its results. It is often used for physical or mathe-

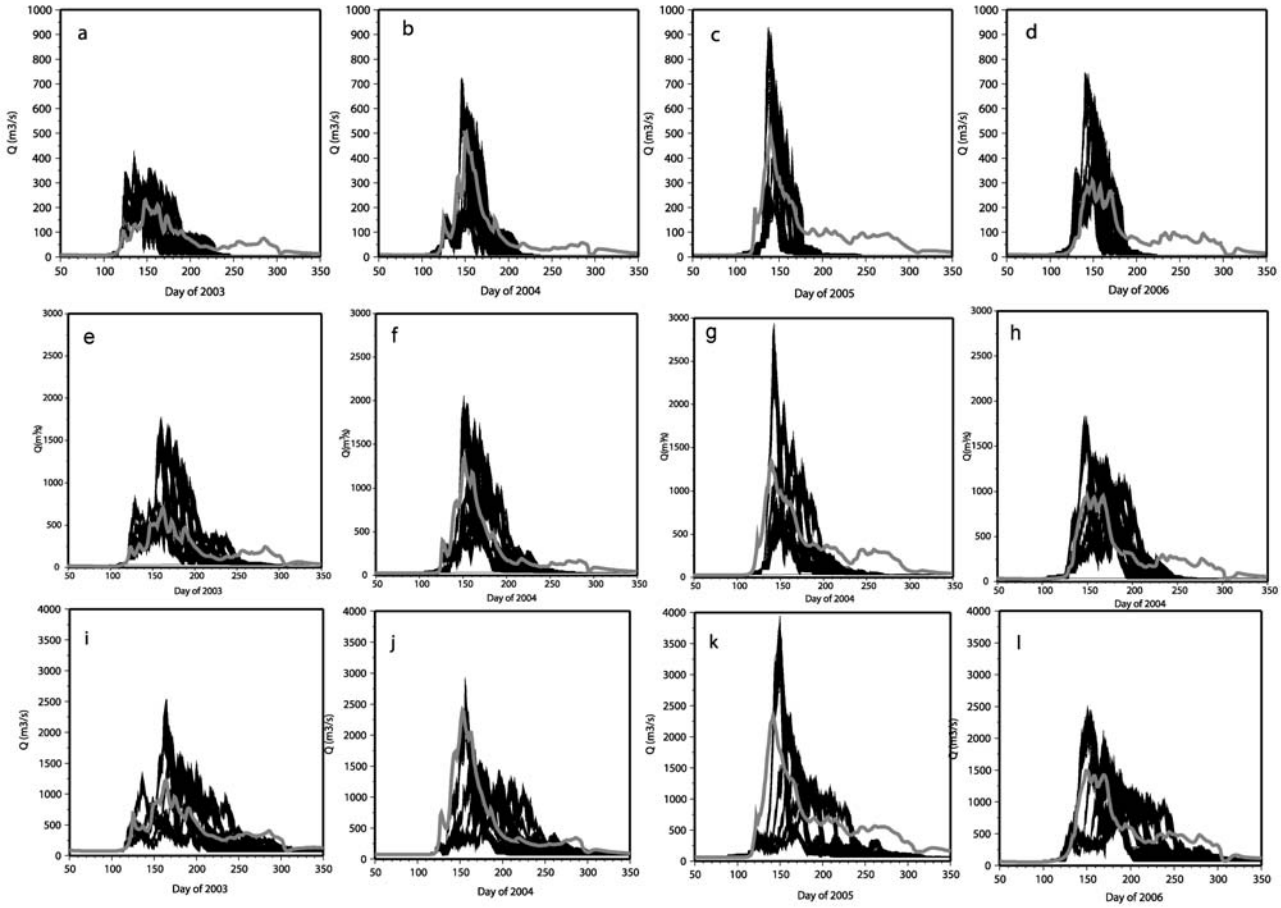

Figure 5. Observed discharge and Monte Carlo discharge simulations using SWEHydro for 2003–2006 at the Ross River at (a–d) Ross River gauge, (e–h) the Pelly River below Vangorda Creek gauge, and (i–l) the Pelly River at Pelly Crossing gauge. Black curves represent the 1000 simulation results. The gray curves are the actual discharge observation at each corresponding gauge.

matical models that are complex or nonlinear or have more than two uncertain parameters that are hard to solve analytically. It is helpful when imitating real life systems or in making predictions (http://vertex42.com/ExcelArticles/mc/MonteCarloSimulation.html). Monte Carlo approaches generally follow a three-step pattern: (1) define the ranges of possible inputs; (2) generate random inputs from the ranges, and then perform deterministic computations on them; and (3) combine each individual computation to obtain the final result [*Metropolis and Ulam*, 1949]. The SWEHydro model has four crucial assumed parameters: smr1, smr2, ft1, ft2. We used the Monte Carlo method to repeat the computation 1000 times to examine how each of these parameters influenced hydrographs in these basins.

[28] Values for the four parameters were randomly generated from certain ranges (Table 4) using the C++ random number generator that produces a uniform distribution. Only integers were used in the Monte Carlo simulations for ft1 and ft2, in order to make sure the output data were in 1 day increments for hydrograph generation and comparison; however, smr1 and smr2 did not have this restriction. The program randomly generated a set of these four parameters within defined ranges and then used them to compute a hydrograph (Figure 5). This step was repeated 1000 times to create 1000 simulations. The program was set up to calculate the best fit to ground observations of discharge and to extract the parameters for the 10 best fits for each year and basin. By doing this, we were able to find the best set of parameters for each year.

[29] We used three criteria to define the best fit to the observations: freshet timing, peak date, and peak discharge magnitude (Figure 6). In Figure 6, the observed discharge for Ross River in 2004 is compared with the best fit curves based on one criterion at a time, freshet timing (Figure 6a), peak timing (Figure 6b), or peak magnitude (Figure 6c). Each of these criteria gets a reasonably good result, and the combination of all three gets the best overall fit (Figure 7). Note that in all cases, the freshet timing is good, even when not optimized. In each of these examples, the peak magnitude is also quite good, although it is not reliable in all years (Figures 5 and 7). Peak timing was better in 2003 and 2004 and less so in 2005 and 2006 (Figures 5 and 7). Notably absent from our model tests is total volume. The total volume of discharge is also an important factor to be considered and correlates with the annual SWE. However, it is still impossible to get a correct mass of snow due to the limitations of the AMSR-E derived SWE estimation for this region. Until SWE retrievals can be refined for this area, this

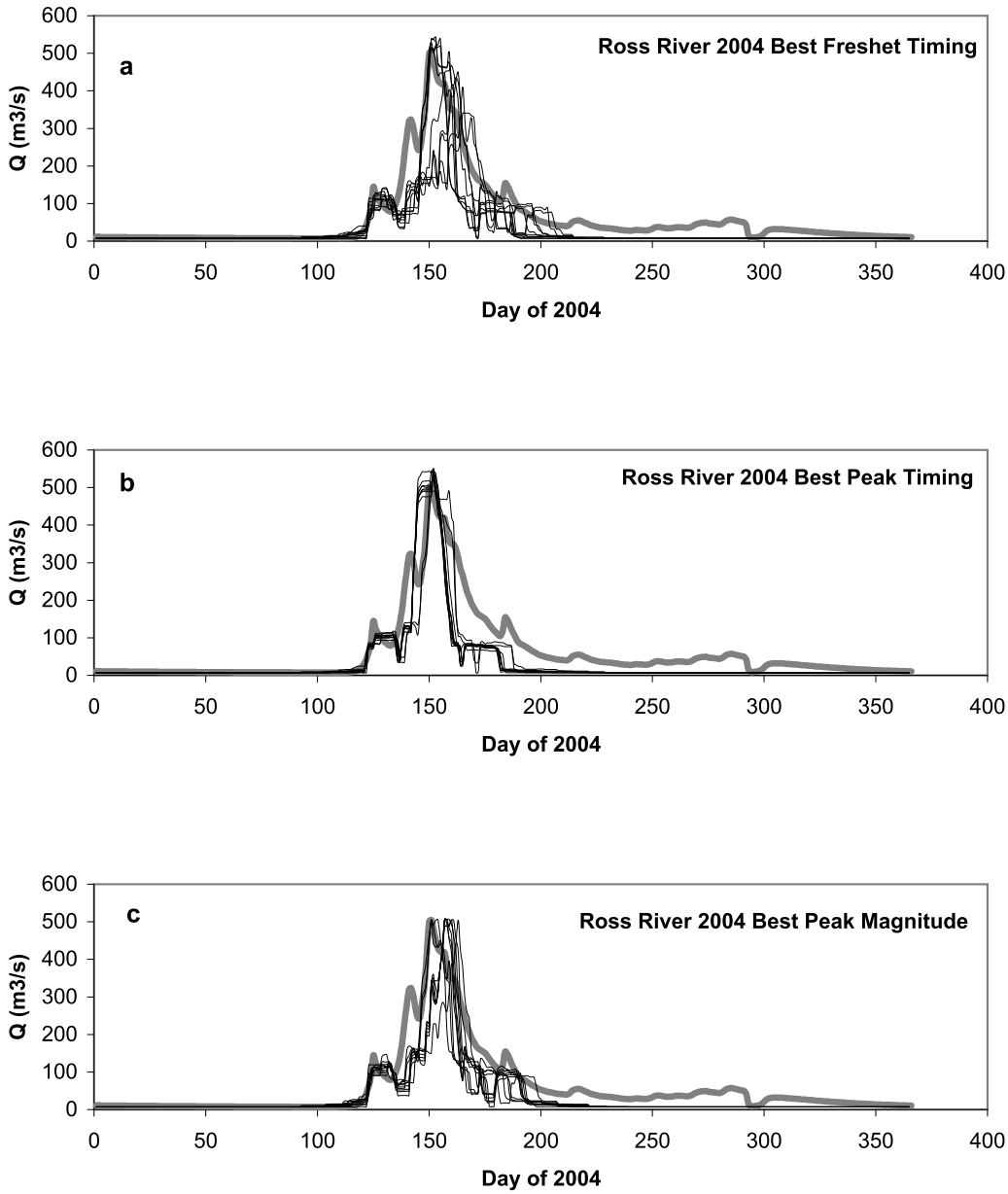

Figure 6. Comparison of 2004 Ross River best fit simulations selected by the (a) best freshet timing, (b) best peak timing, and (c) and best peak magnitude. Black curves are model output. Gray curves are observed discharge.

model performance is not tested against total volume. Groundwater, rainfall, and evaporation also influence the volume of discharge in the stream.

[30] The freshet, or spring snowmelt flood, is defined here as a daily discharge increase that exceeds 20 m^3/s for both the Ross and Pelly rivers. This value is approximated from actual discharge observations from 2003 to 2006. The simulated freshet timing, peak date, and peak discharge were recorded in the program for each simulation to be used to compare with ground-measured discharge.

[31] The best fit selection used a mismatch function [*Björck*, 1996] in order to examine the difference between simulations and observations (Figure 7). The mismatch function for SWEHydro measured the square of the difference between observed and modeled results, and then normalized each. The individual mismatch and total mismatch is shown for Ross River (Table 5) and Pelly River at Pelly Crossing (Table 7). The normalized error function is defined as

$$Error = \frac{(freshet_s - freshet_o)^2}{freshet_o^2} + \frac{(peak_s - peak_o)^2}{peak_o^2} + \frac{(peakmag_s - peakmag_o)^2}{peakmag_o^2}, \quad (4)$$

where $freshet_s$ is simulated freshet timing and $freshet_o$ is observed freshet timing. $Peak_s$ is simulated peak timing and $peak_o$ is observed. $Peakmag_s$ is simulated peak magnitude and $peakmag_o$ is observed. We examined the simulations

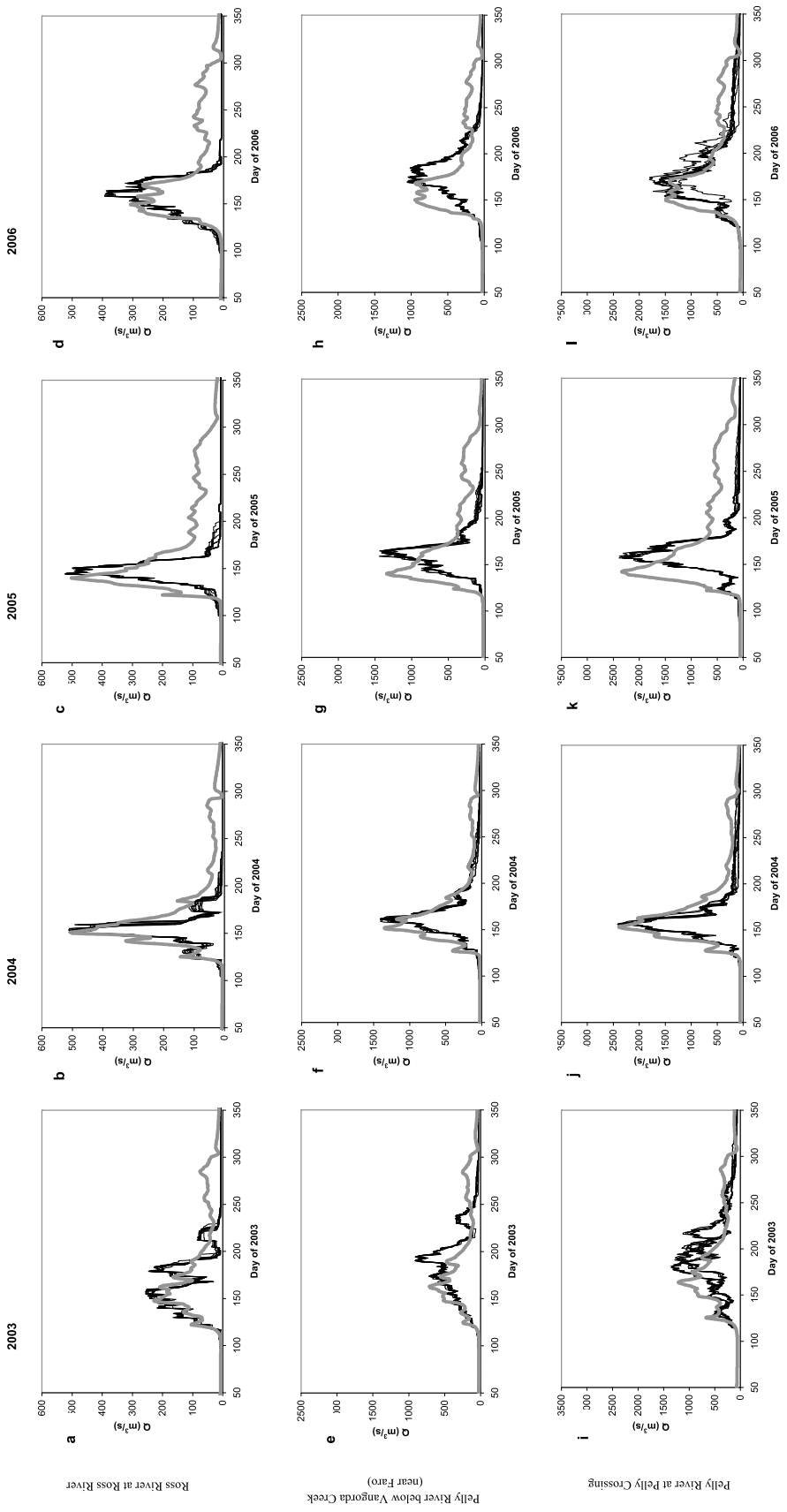

Figure 7. Ten best fit simulations (black curves) compared with actual discharge observations (bold gray curves) for 2003–2006 at (a–d) the Ross River at Ross River gauge, (e–h) the Pelly River below Vangorda Creek gauge, and (i–l) the Pelly River at Pelly Crossing.

Table 5. Hydrograph Characteristics for Simulated Streamflow, Ross River

Hydrograph Characteristics		2003			2004			2005			2006		
		Peak Timing (days)	Peak Magnitude (m^3/s)	Freshet Timing (day)	Peak Timing (days)	Peak Magnitude (m^3/s)	Freshet Timing (day)	Peak Timing (days)	Peak Magnitude (m^3/s)	Freshet Timing (day)	Peak Timing (days)	Peak Magnitude (m^3/s)	Freshet Timing (day)
Observation		148	229	121	151	505	123	140	502	120	149	307	135
Simulations	Minimum	133	249	117	141	337	121	136	351	128	139	382	122
	Maximum	178	430	117	171	724	122	164	928	128	167	746	122
	Mean	147	313	117	157	504	122	147	580	128	153	546	122
Best fits	Minimum	154	249	117	150	500	122	143	504	128	157	382	122
	Maximum	158	256	117	152	510	122	143	522	128	163	391	122
	Mean	156	253	117	151	505	122	143	512	128	160	386	122
Average normalized error[a]		0.00303	0.01111	0.00109	0.00004	0.00007	0.00007	0.00046	0.00058	0.00444	0.00561	0.06682	0.00927

[a]Total error is 0.015 for 2003, 0.00018 for 2004, 0.0055 for 2005, and 0.082 for 2006.

from 2003 to 2006 in detail to see how the best fit parameters changed from year to year (Figures 5, 6, and 7; Tables 6 and 8).

[32] To minimize the effects of poor SWE estimation, we selected the best fit curves by first ranking the top fits for freshet timing, followed by peak timing, and last, peak magnitude which is affected by snow volume (Figure 6; Tables 5 and 7). In this least squares mismatch function, the timing of the freshet (increase) and the peak are both given more weight in our selection process than the peak magnitude because AMSR-E derived snowmelt timing is more accurate than AMSR-E derived SWE. If the model is shown to be a reasonable approximation of reality, the streamflow timing can be obtained correctly from snowmelt timing.

4. Results

4.1. Model Output and Sensitivity Tests

[33] The results of the four sensitivity tests performed on the model are shown in Figure 4. Three of the parameters, smr1 (Figure 4a), smr2 (Figure 4b), and ft1 (Figure 4c) have a small influence on the model output. The flow timing after the melt transition period (ft2) has the greatest control on the model, on both the timing and magnitude (Figure 4d). As ft2 increases, the peak gradually shifts both later and lower. The overall shape of the hydrographs and freshet timing has almost no change in the other three tests, which implies that the variability is not controlled by those assumed parameter values. The second most sensitive parameter is smr2, and it mostly affects peak magnitude. The model is somewhat sensitive to smr1 and insensitive to ft1. It is important to find the best set of parameters to make the simulations fit the real observations. Understanding the factors driving these parameters will also make this model more portable to ungauged basins in the future.

Table 6. Parameters Based on Best Fit Monte Carlo Simulations for Ross River

		2003	2004	2005	2006
Smr1 (mm/d)	Minimum	0.02	0.17	0.83	0.54
	Maximum	0.84	0.96	0.98	0.99
	Mean	0.25	0.60	0.92	0.84
Smr2 (mm/d)	Minimum	8.02	8.14	9.77	8.74
	Maximum	10.79	10.12	10.26	9.80
	Mean	9.96	8.76	10.04	9.33
Ft1 (days)	Minimum	6	6	6	6
	Maximum	10	10	10	9
	Mean	8.3	8.5	7.4	7.6
Ft2 (days)	Minimum	5	2	3	5
	Maximum	5	2	3	5
	Mean	5.0	2.0	3.0	5.0

4.2. Monte Carlo Simulations

[34] For the Ross River basin (Figures 7a–7d), the 10 best simulations for 2003 (Figure 7a) and 2004 (Figure 7b) are very close to actual observations. They have similar freshet timing and peak timing and magnitude as well as similar hydrograph shapes. For 2005 (Figure 7c), the model flow does not match freshet timing: The simulations lag 8 days compared with the real observations. For 2006 (Figure 7d), peak magnitudes and hydrograph shape are poor fits. The poor fits show us the areas for improvement in the model and will be used to refine it as it is applied in additional basins and years. The simulation statistics are shown in Table 5. The 2004 simulation has the smallest error (0.00015), while the 2006 simulation has the largest (0.082).The values in Table 6 are the minimum, maximum, and mean values of each parameter for the 10 best simulations. These differ from year to year, which is reasonable because they are affected by the annual snow distribution and mass variability and the conditions controlling melt rates. This natural variability makes it much harder to establish the best way to use the model in other basins, at least until we know more about the landscape, snowpack, and model factors that drive the variations. We are developing a future study to determine which variations are controlled by the basin (topography, channel characteristics, land cover, and permafrost, for example) and which are related to the atmosphere and snowpack characteristics and are variable on a daily and annual basis.

[35] For the Pelly River basin (gauges at Faro and Pelly Crossing), the 1000 simulations vary significantly (Figures 5e–5l), which implies that the parameter combinations affect the hydrographs differently. The 10 best fit simulations for each gauge are also selected based on freshet timing, peak location, and peak magnitude (Figures 7e–7l). Similar to the Ross River basin, the freshet timing is consistent. The average of freshet dates for 2003 to 2006 is within 5 days of the real observations. However, the simulations for peak timing and magnitude are not as good. The 10 best simulations from 2003 to 2006 are shown in

Table 7. Hydrograph Characteristics for Simulated Streamflow, Pelly River

Hydrograph Characteristics		2003			2004			2005			2006		
		Peak Timing (days)	Peak Magnitude (m^3/s)	Freshet Timing (day)	Peak Timing (days)	Peak Magnitude (m^3/s)	Freshet Timing (day)	Peak Timing (days)	Peak Magnitude (m^3/s)	Freshet Timing (day)	Peak Timing (days)	Peak Magnitude (m^3/s)	Freshet Timing (Day)
Observation		164	1210	119	153	2390	123	142	2340	117	149	1490	128
Simulations	Minimum	160	1160	114	155	927	120	147	987	112	150	1020	119
	Maximum	204	2538	114	232	2930	120	213	3948	116	218	2501	126
	Mean	180	1616	114	187	1494	120	168	1912	114	178	1614	123
Best fits	Minimum	179	1192	114	155	2376	120	156	2251	113	166	1521	121
	Maximum	188	1349	114	155	2406	120	157	2383	113	175	1702	123
	Mean	184	1293	114	155	2393	120	156	2301	113	169	1633	121
Average normalized error[a]		0.01465	0.00668	0.00177	0.00017	0.00001	0.00060	0.01001	0.00055	0.00116	0.01833	0.01051	0.00284

[a]Total error is 0.023 for 2003, 0.00078 for 2004, 0.011 for 2005, and 0.032 for 2006.

Figure 7. Simulation statistics for the Pelly River at Pelly Crossing gauge are listed in Table 7.

[36] For the upper Pelly River, gauged below Vangorda Creek, 2003 and 2004 show good agreement with freshet timing, and reasonable but not perfect peak timing and magnitude (Figures 7e and 7f). In 2005, the model is not very close to the observations in freshet date or peak timing (Figure 7g). This was a large, rapid spring flood based on the hydrometric results and ground observations, which shows us that the model does not account for very rapid melt rates or increases in flow timing, something that a meteorologically based model might do better in this case. The year 2006 shows freshet timing and magnitude to be reasonable, but the Pelly River has a long drawn out peak that precedes the model peak (Figure 7h).

[37] In the whole Pelly River basin, the best fits for 2003 (Figure 7i–7l) have hydrographs shaped similarly to the observations, indicating the effectiveness of the SWEHydro model. In 2003, the overall shape is good, as is freshet timing and peak magnitude. There were multiple subdued peaks in this year, and the model did capture that pattern, although the timing is not perfect. The best fits for 2004 (Figure 7j) match the real situation well and have the smallest error (0.00078). For 2005 (Figure 7k), the early, large freshet decreased the fit. The simulations for 2006 (Figure 7l) have the largest overall error, although freshet timing and peak magnitude are quite similar. Peak timing was the worst performer in 2006. Table 8 lists the optimal parameters for the Pelly River basin gauged at Pelly Crossing from 2003 to 2006. The parameters used for the best fit curves vary within the allowed ranges. Refining these parameters so that they represent the basin characteristics in a general way will be necessary to estimate flow ranges in advance and eventually to apply the model to future scenarios or ungauged basins. Subsequent steps include applying the model to additional years and to other basins with controlled differences by varying one major characteristic at a time.

Table 8. Parameters Based on Best Fit Monte Carlo Simulations for Pelly River

		2003	2004	2005	2006
Smr1 (mm/d)	Minimum	0.59	0.17	0.05	0.79
	Maximum	0.99	0.71	0.75	0.99
	Mean	0.88	0.54	0.40	0.91
Smr2 (mm/d)	Minimum	8.44	8.28	11.39	8.09
	Maximum	11.99	12.00	11.98	11.56
	Mean	9.96	10.37	11.81	9.68
Ft1 (days)	Minimum	7	6	6	7
	Maximum	10	10	10	10
	Mean	8.5	7.7	8.2	9.1
Ft2 (days)	Minimum	3	1	2	2
	Maximum	4	1	2	3
	Mean	3.5	1.0	2.0	2.1

5. Discussion

[38] The SWEHydro model was developed as a simple way to characterize streamflows in snow-dominated regions with limited meteorological information used to drive more conventional models. It uses SWE observations from passive microwave as the input snow mass and melt characterization and timing information to infer when and how much the snowpack is melting. It was evaluated for the Pelly River and its subbasin, the Ross River. Because no meteorological data are expected by the model, it needs to estimate the melt rates at different parts of the melt season. When the snow has just started to melt, and continues to freeze during the night (transition season), the melt rates are, on average, low. After the transition season, the melt rates increase and there is little refreezing overnight; the snowpack is ripe and flow rates also increase. The user controls the range of possible values, and they are randomly selected within the specified range by a Monte Carlo process. For these gauged basins, best fits are selected based on ground-based streamflow. We do not fully understand the governing processes that are represented by the model parameters other than to say that we do know how model output is sensitive to parameter changes. Once the model and parameter characteristics are well understood, it may be possible to use it to predict a window of possible flow characteristics without ground-based observations.

[39] We evaluated the sensitivity to each of the four parameters. For the four assumed parameters in the SWEHydro model, the snowmelt rate (smr1) and flow timing (ft1) during the melt transition have limited influences on the hydrographs (Figures 4a and 4c). The variation of snowmelt rate after the transition period (smr2) affected the peak magnitude (Figure 4b). The faster the snowpack melts, the higher the peak magnitude appears on the hydrograph. The variation of ft2 affected both the peak timing and magnitude (Figure 4d) and had the largest effect on the

model of all the parameters. A large value for ft2, which means water flows slowly on the ground or through the near surface, would cause a later peak time and a lower peak magnitude compared with a small ft2. We compared the average ft2 for the 10 best fit curves to observed peak magnitude, and there is an inverse relationship ($R^2 = 0.7$). In high peak flow years, ft2 is lower. When maximum ft2 of the 10 best fits is compared with mean SWE (mean pixel SWE for the Pelly basin was 131, 111, 123, and 143 mm in 2003, 2004, 2005, and 2006, respectively), there is a correlation ($r^2 = 0.6$) suggesting that in higher snow years, ft2 will increase. Thus we infer that the higher snow mass buffers melt, possibly somewhat independently of climatic conditions. This is consistent with snowpack thermal inertia and the (generally) rapid transition from $-20°C$ to near freezing in the region. This complexity embedded in the ft2 parameter means that increased snow does not automatically mean faster delivery to the channel. These relationships suggest that ft2 encompasses a varied set of processes, related to snow quantity and strongly influenced by the surface processes that control how fast it gets to the gauge (which may themselves be influenced by snow distribution and quantity). This is consistent with the significance and variability observed in this and other northern watersheds [e.g., *Woo*, 2008; *Marsh et al.*, 2008]. The freshet timing does not have much variation as a result of changes of assumed parameters, which implies that it is not controlled by these parameters; it is affected primarily by the snowmelt timing extracted from satellite data. The model is therefore an effective predictor of freshet timing.

[40] The statistics of simulated parameters used for best fits can also show their influence on the hydrographs. The maximum and minimum smr1, smr2, and ft1 vary greatly, sometimes from the low boundary of the simulation ranges to the high boundary. Ft2 does not have much variation, though. Ft2 is the flow timing after the transition period, which directly relates to the peak date on the hydrographs. Most of the maximum and minimum ft2 values for individual years are the same, which means all the best 10 fits used the same ft2 in the SWEHydro model (Tables 6 and 8). This is consistent with the sensitivity tests. Parameter ft2 has the greatest influence on the hydrographs, so the values used in the best fits should not differ much.

[41] SWEHydro accurately predicts freshet timing, and with the exception of years of very rapid runoff, seems to get the initial freshet magnitude correct. The flow timing 2 parameter, which is important for estimating modeled stream discharge peak timing and magnitude, varies from year to year and basin to basin. This means there is a need to understand the terrain and snowpack characteristics controlling the flow timing in order to develop the SWEHydro model into an effective and reliable predictor of peak timing and magnitude.

6. Conclusions

[42] As global warming continues to melt snowpacks earlier and faster in the high-latitude regions [e.g., *Serreze et al.*, 2000; *Arctic Climate Impact Assessment* (*ACIA*), 2004, 2005; *Intergovernmental Panel on Climate Change* (*IPCC*), 2007], accurate monitoring of snowmelt runoff in inaccessible arctic and subarctic areas will become increasingly important. This study shows that AMSR-E passive microwave data observations are a simple but powerful tool to investigate snowmelt timing, snow water equivalent (SWE), and their collective effects on streamflow timing and magnitude in high-latitude regions, specifically the upper Yukon River basin. The SWEHydro model, developed to use solely remote sensing observations and DEM data, is effective in simulating spring stream freshet and peak timing and magnitude in basins lacking sufficient available in situ weather measurements for conventional models. The sensitivity tests demonstrate that the simulated freshet timing is strongly related to the AMSR-E derived snowmelt timing, and that the modeled hydrograph is strongly dependent on the flow timing parameter, which is sensitive to the amount of snow, temporally variable terrain characteristics such as ponding, and static terrain characteristics. This model is being refined for use identifying potential snowmelt-driven spring floods in inaccessible high-latitude or mountainous regions and ungauged watersheds. Because the assumed parameters are partly related to the local weather conditions for specific year, the model can also be regarded as a tool for risk assessment, which can give a probability that the peak discharge would exceed a certain safe standard. The next logical step is to apply the SWEHydro model to other, undammed and gauged drainages to (1) reproduce the result for the Pelly River in basins with similar size, topography, geology, and land cover, and (2) explore the results for basins of variable size, topography, geology or land cover to begin to isolate the constitutive processes governing the flow timing parameter. Future model improvements include improving accuracy of SWE estimation by using high-resolution 12.5×12.5 km AMSR-E SWE data and a region-specific algorithm, incorporating groundwater effects, and refining snowmelt rates and flow timing estimations. Improved flow paths will incorporate more detailed topography. Finally, we plan to test the model in basins with a range of terrain characteristics in order to develop techniques to constrain the parameters used in this model for ungauged basins. Ultimately, we hope to apply the SWEHydro model to other arctic and subarctic watersheds to assist in studies of water resource variability and climate change.

[43] **Acknowledgments.** We thank NSIDC and NASA/NASDA for use of the AMSR-E L2A and L3 data and Environment Canada for the stream discharge data. We thank the Yukon Territorial Government for the digital elevation model (Environment Yukon), and Glenn Ford, Richard Janowicz, and the YTG Hydrology Branch for snow pillow data. We are grateful to Pat Maltais, Sarah Kopczynski, Beth Lambert, Jeremy Apgar, and Ken Karnas for their assistance in collecting data in the Yukon. This research was supported by the NASA grant NNG04GR31G and Lehigh University. Richard Weisman, Frank Pazzaglia, Zicheng Yu, Benjamin Felzer, Richard Kelly, three anonymous reviewers, and *Water Resources Research* editors provided helpful discussions and suggestions to improve the manuscript.

References

Aagaard, K., and E. C. Carmack (1989), The role of sea ice and other fresh water in the Arctic circulation, *J. Geophys. Res.*, *94*(C10), 14,485–14,498, doi:10.1029/JC094iC10p14485.

Apgar, J. D., J. Ramage, R. McKenney, and P. Maltais (2007), AMSR-E algorithm for snowmelt onset detection in sub-arctic heterogeneous terrain, *Hydrol. Processes*, *21*(12), 1587–1596, doi:10.1002/hyp.6721.

Arctic Climate Impact Assessment (ACIA) (2004), *Impacts of a Warming Arctic: Synthesis Report*, 29 pp., Cambridge Univ. Press, New York.

Arctic Climate Impact Assessment (ACIA) (2005), *Impacts of a Warming Arctic: Scientific Report*, 1046 pp., Cambridge Univ. Press, New York.

Armstrong, R. L., and M. J. Brodzik (2001), Recent Northern Hemisphere snow extent: A comparison of data derived from visible and microwave satellite sensors, *Geophys. Res. Lett.*, *28*(19), 3673–3676, doi:10.1029/2000GL012556.

Ashcroft, P., and F. Wentz (2003), AMSR-E/Aqua L2A global swath spatially-resampled brightness temperatures (Tb) V001, January 2003 to December 2006, Natl. Snow and Ice Data Cent., Boulder, Colo.

Björck, A. (1996), *Numerical Methods for Least Squares Problems*, Cambridge Univ. Press, New York.

Brabets, T. P., B. Wang, and R. H. Meade (2000), Environmental and hydrologic overview of the Yukon River Basin, Alaska and Canada, *U.S. Geol. Surv. Water Resour. Invest. Rep., 99-4204*, 106 pp.

Chang, A. T. C., and P. Gloersen (1975), Microwave emission from dry and wet snow, in *Operational Applications of Satellite Snowcover Observations*, edited by A. Rango, *NASA, Spec. Publ., SP-391*, 399–407.

Chang, A. T. C., P. Gloersen, T. Schmugge, T. T. Wilheit, and H. J. Zwally (1976), Microwave emission from snow and glacier ice, *J. Glaciol.*, *16*, 23–39.

Chang, A. T. C., J. L. Foster, D. K. Hall, A. Rango, and B. Hartline (1982), Snow water equivalence determination by microwave radiometry, *Cold Reg. Sci. Technol.*, *5*, 259–267, doi:10.1016/0165-232X(82)90019-2.

Chang, A. T. C., J. L. Foster, and D. K. Hall (1987), Nimbus-7 SMMR derived global snow cover parameters, *Ann. Glaciol.*, *9*, 39–45.

Chang, A. T. C., J. L. Foster, D. K. Hall, B. E. Goodison, A. E. Walker, and J. R. Metcalfe (1997), Snow parameters derived from microwave measurements during the BOREAS winter field experiment, *J. Geophys. Res.*, *102*, 29,663–29,671, doi:10.1029/96JD03327.

Chang, A. T. C., R. E. J. Kelly, J. L. Foster, and D. K. Hall (2003), Global SWE monitoring using AMSR-E data, in *Geoscience and Remote Sensing Symposium, 2003: IGARSS '03, Proceedings, 2003 IEEE International*, vol. 1, pp. 680–682, IEEE Press, New York.

Derksen, C., A. Walker, and P. Toose (2008), Estimating snow water equivalent in northern regions from satellite passive microwave data, in *Cold Region Atmospheric and Hydrologic Studies: The Mackenzie GEWEX Experience*, vol. 1, pp. 195–212, Springer, New York.

Dewey, K. F., and R. Heim Jr. (1981), Satellite observations of variations in Northern Hemisphere seasonal snow cover, *NOAA Tech. Rep., NESS- 87*, 85 pp.

Dong, J., J. P. Walker, and P. R. Houser (2005), Factors affecting remotely sensed snow water equivalent uncertainty, *Remote Sens. Environ.*, *97*(1), 68–82, doi:10.1016/j.rse.2005.04.010.

Foster, J. L., A. T. C. Chang, D. K. Hall, and A. Rango (1991), Derivation of snow water equivalent in boreal forests using microwave radiometry, *Arctic*, *44*(1), 147–152.

Goodison, B., A. E. Walker, and F. W. Thirkettle (1990), Determination of snowcover on the Canadian prairies using passive microwave data, paper presented at the International Symposium on Remote Sensing and Water Resources, Enschede, Netherlands, 20–24 Aug.

Grebmeier, J. M., J. E. Overland, S. E. Moore, E. V. Farley, E. C. Carmack, L. W. Cooper, K. E. Frey, J. H. Helle, F. A. McLaughlin, and S. L. McNutt (2006), A major ecosystem shift in the northern Bering Sea, *Science*, *311*(5766), 1461–1464, doi:10.1126/science.1121365.

Hall, D. K., M. Sturm, C. S. Benson, A. T. C. Chang, J. L. Foster, H. Garbeil, and E. Chacho (1991), Passive microwave remote sensing within a mountainous subarctic watershed, in *Proceedings of the 59th Annual Eastern Snow Conference*, pp. 67–81, Stowe, Vt.

Hallikainen, M. T., and P. A. Jolma (1986), Retrieval of water equivalent of snow cover in Finland by satellite microwave radiometry, *IEEE Trans. Geosci. Remote Sens., GE*, *24*(6), 855–862, doi:10.1109/TGRS.1986.289700.

Hansen, M., R. DeFries, J. R. Townshend, M. Carroll, C. Dimiceli, and R. Sohlberg (2003), 500m MODIS vegetation continuous fields, Global Land Cover Facil., College Park, Md.

Intergovernmental Panel on Climate Change (IPCC) (2007), *Climate Change 2007: Synthesis Report—Contribution of Working Groups I, II and III to the Fourth Assessment Report of the Intergovernmental Panel on Climate Change*, edited by P. K. Pachauri and A. Reisinger, 104 pp., Geneva, Switzerland.

Kawanishi, T., T. Sezai, Y. Ito, K. Imaoka, T. Takeshima, Y. Ishido, A. Shibata, M. Miura, H. Inahata, and R. W. Spencer (2003), The Advanced Microwave Scanning Radiometer for the Earth Observing System (AMSR-E), NASDA's contribution to the EOS for global energy and water cycle studies, *IEEE Trans. Geosci. Remote Sens.*, *41*(2), 184–194, doi:10.1109/TGRS.2002.808331.

Kelly, R. E., A. T. C. Chang, L. Tsang, and J. L. Foster (2003), A prototype AMSR-E global snow area and snow depth algorithm, *IEEE Trans. Geosci. Remote Sens.*, *41*(2), 230–242, doi:10.1109/TGRS.2003.809118.

Kelly, R. E. J., A. T. C. Chang, and J. L. Foster (2004), AMSR-E/Aqua daily L3 global snow water equivalent EASE-Grids, V001, January 2003 to December 2006, Natl. Snow and Ice Data Cent., Boulder, Colo.

Kunzi, K. F., S. Patil, and H. Rott (1982), Snow-cover parameters retrieved from Nimbus-7 scanning multichannel microwave radiometer (SMMR) data, *IEEE Trans. Geosci. Remote Sens.*, *GE-20*(4), 452–467, doi:10.1109/TGRS.1982.350411.

Liston, G. E. (1999), Interrelationships among snow distribution, snowmelt, and snow cover depletion: Implications for atmospheric, hydrologic, and ecologic modeling, *J. Appl. Meteorol.*, *38*, 1474–1487, doi:10.1175/1520-0450(1999)038<1474:IASDSA>2.0.CO;2.

MacKay, M. D., P. A. Bartlett, E. Chan, C. Derksen, S. Guo, and H. Leighton (2006), On the simulation of regional scale sublimation over boreal and agricultural landscapes in a climate model, *Atmos. Ocean*, *44*, 289–304, doi:10.3137/ao.440306.

Marsh, P., J. Pomeroy, S. Pohl, W. Quinton, C. Onclin, M. Russell, N. Neumann, A. Pietroniro, B. Davison, and S. McCartney (2008), Snowmelt processes and runoff at the Arctic treeline: Ten years of MAGS research, in *Cold Region Atmospheric and Hydrologic Studies: The Mackenzie GEWEX Experience*, vol. 2, *Hydrologic Processes*, edited by M. Woo, pp. 97–123, Springer, New York.

Martinec, J., and A. Rango (1986), Parameter values for snowmelt runoff modeling, *J. Hydrol.*, *84*, 197–219, doi:10.1016/0022-1694(86)90123-X.

Mätzler, C. (1987), Applications of the interaction of microwaves with the natural snow cover, *Remote Sens. Rev.*, *2*, 259–391.

Metropolis, N., and S. Ulam (1949), The Monte Carlo method, *J. Am. Stat. Assoc.*, *44*, 335–341, doi:10.2307/2280232.

Ramage, J. M., R. A. McKenney, B. Thorson, P. Maltais, and S. E. Kopczynski (2006), Relationship between passive microwave-derived snowmelt and surface-measured discharge, Wheaton River, Yukon Territory, Canada, *Hydrol. Processes*, *20*(4), 689–704, doi:10.1002/hyp.6133.

Ramage, J. M., J. D. Apgar, R. A. McKenney, and W. Hanna (2007), Spatial variability of snowmelt timing from AMSR-E and SSM/I passive microwave sensors, Pelly River, Yukon Territory, Canada, *Hydrol. Processes*, *21*, 1548–1560, doi:10.1002/hyp.6717.

Schmugge, T. J., W. P. Kustas, J. C. Ritchie, T. J. Jackson, and A. Rango (2002), Remote sensing in hydrology, *Adv. Water Resour.*, *25*, 1367–1385, doi:10.1016/S0309-1708(02)00065-9.

Serreze, M. C., J. E. Walsh, F. S. Chapin III, T. Osterkamp, M. Dyurgerov, V. Romanovsky, W. C. Oechel, J. Morison, T. Zhang, and R. G. Barry (2000), Observational evidence of recent change in the northern high-latitude environment, *Clim. Change*, *46*, 159–207, doi:10.1023/A:1005504031923.

Sturm, M., J. Holmgren, and G. E. Liston (1995), A seasonal snow cover classification system for local to global applications, *J. Clim.*, *8*, 1261–1283, doi:10.1175/1520-0442(1995)008<1261:ASSCCS>2.0.CO;2.

Tedesco, M. (2007), Snowmelt detection over the Greenland ice sheet from SSM/I brightness temperature daily variations, *Geophys. Res. Lett.*, *34*, L02504, doi:10.1029/2006GL028466.

U.S. Army Corps of Engineers (1956), Snow hydrology: Summary report on the snow investigations, N. Pac. Div., Portland, Oreg.

Walker, A. E., and B. E. Goodison (1993), Discrimination of a wet snow cover using passive microwave satellite data, *Ann. Glaciol.*, *17*, 307–311.

Woo, M. (Ed.) (2008), *Hydrologic Processes*, vol. 2, 507 pp., Springer, New York.

Woo, M. K., and R. Thorne (2006), Snowmelt contribution to discharge from a large mountainous catchment in subarctic Canada, *Hydrol. Processes*, *20*, 2129–2139, doi:10.1002/hyp.6205.

R. McKenney, Department of Geosciences/Environmental Studies, Pacific Lutheran University, Tacoma, WA 98447, USA.

J. Ramage and F. Yan, Earth and Environmental Sciences Department, Lehigh University, Bethlehem, PA 18015, USA. (ramage@lehigh.edu)